Biomedicine & Pharmacotherapy 156 (2022) 113947

Contents lists available at ScienceDirect

Biomedicine & Pharmacotherapy

journal homepage: www.elsevier.com/locate/biopha

Empagliflozin reduces kidney fibrosis and improves kidney function by alternative macrophage activation in rats with 5/6-nephrectomy

Yong-Ping Lu [a,1], Hong-Wei Wu [a,1], Ting Zhu [a,1], Xi-Tong Li [b], Jiao Zuo [b], Ahmed A. Hasan [b,c], Christoph Reichetzeder [d], Denis Delic [b,e], Benito Yard [b], Thomas Klein [e], Bernhard K. Krämer [b,f,g], Ze-Yu Zhang [h], Xiao-Hua Wang [a], Liang-Hong Yin [h], Yong Dai [i,*], Zhi-Hua Zheng [a,**], Berthold Hocher [b,j,k,l,***]

[a] Department of Nephrology, Center of Kidney and Urology, the Seventh Affiliated Hospital, Sun Yat-sen University, Shenzhen, China
[b] Fifth Department of Medicine (Nephrology/Endocrinology/Rheumatology/ Pneumology), University Medical Centre Mannheim, University of Heidelberg, Germany
[c] Institute of Pharmacy, Free University of Berlin, Berlin, Germany
[d] HMU – Health and Medical University, Potsdam, Germany
[e] Boehringer Ingelheim Pharma GmbH & Co. KG, Biberach, Germany
[f] European Center for Angioscience ECAS, Medical Faculty Mannheim of the University of Heidelberg, Mannheim, Germany
[g] Mannheim Center for Innate Immunoscience, Medical Faculty Mannheim of the University of Heidelberg, Mannheim, Germany
[h] Department of Nephrology, the First Affiliated Hospital of Jinan University, Guangzhou, China
[i] The Second Clinical Medical College of Jinan University, Shenzhen People's Hospital, Shenzhen, China
[j] Reproductive and Genetic Hospital of CITIC-Xiangya, Changsha, China
[k] Key Laboratory of Stem Cells and Reproductive Engineering, Ministry of Health, Changsha, China
[l] Institute of Medical Diagnostics, IMD, Berlin, Germany

ARTICLE INFO

Keywords:
Non-diabetic kidney disease
SGLT2 inhibitor
Macrophage-myofibroblast transition
Fibrosis
Polarization

ABSTRACT

Background: Sodium glucose cotransporter 2 (SGLT2) inhibitors originally developed for the treatment of type 2 diabetes are clinically very effective drugs halting chronic kidney disease progression. The underlying mechanisms are, however, not fully understood.

Methods: We generated single-cell transcriptomes of kidneys from rats with 5/6 nephrectomy before and after SGLT2 inhibitors treatment by single-cell RNA sequencing.

Findings: Empagliflozin treatment decreased BUN, creatinine and urinary albumin excretion compared to placebo by 39.8%, 34.1%, and 55%, respectively ($p < 0.01$ in all cases). Renal interstitial fibrosis and glomerulosclerosis was likewise decreased by 51% and 66.8%; respectively ($p < 0.05$ in all cases). 14 distinct kidney cell clusters could be identified by scRNA-seq. The polarization of M2 macrophages from state 1 ($CD206^-CD68^-$ M2 macrophages) to state 5 ($CD206^+CD68^+$ M2 macrophages) was the main pro-fibrotic process, as $CD206^+CD68^+$ M2 macrophages highly expressed fibrosis-promoting genes and can convert into fibrocytes. Empagliflozin remarkably inhibited the expression of fibrosis-promoting (*IFG1* and *TREM2*) and polarization-associated genes (*GPNMB, LGALS3*, *PRDX5*, and *CTSB*) in $CD206^+CD68^+$ M2 macrophages and attenuated inflammatory signals from $CD8^+$ effector T cells. The inhibitory effect of empagliflozin on $CD206^+CD68^+$ M2 macrophages polarization was mainly achieved by affecting mitophagy and mTOR pathways.

Interpretation: We propose that the beneficial effects of empagliflozin on kidney function and morphology in 5/6 nephrectomyiced rats with established CKD are at least partially due to an inhibition of $CD206^+CD68^+$ M2

* Correspondence to: The First Affiliated Hospital of Southern University of Science and Technology, the Second Clinical Medical College of Jinan University, Shenzhen People's Hospital, Shenzhen 518020, China.
** Corresponding author.
*** Correspondence to: Fifth Department of Medicine (Nephrology/Endocrinology/Rheumatology/Pneumology), University Medical Centre Mannheim, University of Heidelberg, Theodor-Kutzer-Ufer 1-3, 68167 Mannheim, Germany.
E-mail addresses: daiyong22@aliyun.com (Y. Dai), zhihuazheng@126.com, zhzhihua@mail.sysu.edu.cn (Z.-H. Zheng), berthold.hocher@medma.uni-heidelberg.de (B. Hocher).
[1] Yong-Ping Lu, Hong-Wei Wu and Ting Zhu contributed equally to this work.

https://doi.org/10.1016/j.biopha.2022.113947
Received 17 August 2022; Received in revised form 20 October 2022; Accepted 28 October 2022
Available online 31 October 2022

macrophage polarization by targeting mTOR and mitophagy pathways and attenuating inflammatory signals from $CD8^+$ effector T cells.
Fundings: A full list of funding bodies that contributed to this study can be found in the Acknowledgements section.

1. Introduction

The primary effect of sodium glucose cotransporter 2 inhibitors (SGLT2i) is the reduction of blood glucose by an inhibition of glucose and sodium reabsorption in the proximal tubulus [1]. However, already in the first cardiovascular safety trial, the EMPA-REG OUTCOME trial, a very clear benefit regarding the protection against major adverse cardiovascular and renal events was seen [1,2]. Similar results were obtained by following studies of other SGLT2 inhibitors [3,4]. Furthermore, the CREDENCE trial, the first trial primarily focusing on renal outcomes, was able to demonstrate a substantial relative risk reduction of the composite renal endpoint [5]. The DAPA-CKD trial was halted prematurely because of the overwhelming efficacy of dapagliflozin in risk reduction for the composite endpoint of a sustained decline of eGFR, end stage kidney disease, or death from renal or cardiovascular causes [6,7].

However, the very effective mechanisms of kidney protection by SGLT2 inhibition, a drug class originally developed for the treatment of type 2 diabetes, remain unclear. One important reno-protective mechanism is the restoration of the tubuloglomerular feedback mechanisms [8]. Hyperglycemia, leading to an increase in proximal tubule glucose filtered load, causes SGLT2 overactivity with an increased reabsorption of glucose and sodium in the proximal tubule. This increased sodium reabsorption causes a decrease of sodium levels at the macula densa, diminishing adenosine secretion. Lack of adenosine, a strong vasoconstrictor, triggers vasodilatation of the afferent arteriole and thus hyperfiltration [9]. SGLT2 inhibition in turn leads to increased sodium concentrations at the macula densa, vasoconstriction at the afferent arteriole which counteracts glomerular hyperfiltration and thus elicits renoprotective effects [8]. However, as this mechanism mainly is based on alleviating homeostatic disturbances due to hyperglycemia, crucial renoprotective mechanisms by SGLT2 inhibition in non-diabetic CKD remain to be identified. Currently the elucidation of relevant mechanisms is subject of many investigations and it was shown that SGLT2 inhibitors display a range of pleiotropic effects, ranging from modulation of the renin-angiotensin-aldosterone system, changes in energy substrate usage, anti-oxidative, anti-inflammatory and to some extent immune modulatory effects [7,10–12]. Our own recent study even provides evidence that the TGF mechanisms does not play a key role in non-diabetic CKD [13].

The aim of the current study was to investigate the effects of empagliflozin in a 5/6 nephrectomy rats, a well-established model of non-diabetic CKD. To be able to characterize renal effects of empagliflozin on an individual cell level and get a better insight regarding putative reno-protective mechanisms, the single-cell RNA sequencing was employed. Single-cell RNA sequencing (scRNA-seq) is an emerging technology, that allows investigators to assess global gene regulation in thousands of single cells in an unbiased and reproducible manner. The application of single-cell technologies has become a viable tool in the investigation of cellular heterogeneity, transcriptomic signatures, and molecular dynamics of kidney diseases, and assists in the characterisation of pathological mechanisms and counteracting drug effects [14,15].

2. Methods

2.1. Chronic kidney disease model (5/6 nephrectomies rats)

The Wistar rats were housed in a specific pathogen-free animal house at Jinan University's animal experimental center, with a constant temperature (24 ± 1) ℃ and a 12/12 light cycle. The animal experiment was approved by Jinan University's institutional animal care and use committee (NO. 00245787) and carried out in accordance laboratory animals care and use norms.

A total of 22 pathogen-free, 6- to 7- week-old male wistar rats weighing 200–250 g were divided into three groups: sham + placebo (Sham group, n = 7); 5/6 Nx + placebo (5/6Nx group, n = 6); 5/6 Nx + placebo + empagliflozin (Empa group, n = 9). The 5/6 Nx operations were performed as follows [16]: the upper and lower poles of the left kidney were amputated at week 2, followed by excision of the right kidney at week 4. This model allowed for the removal of approximately 5/6 of the kidney while preserving a tiny portion of functioning renal parenchyma to mimic the condition of CKD. Sham operations were conducted at the same time points and merely executed laparotomy. All animals were anesthetized with intraperitoneal injection of 20 mg/ml 3, 3,3-tribromoethanol (dosage: 300–400 mg/kg) while producing 5/6 Nx. Empagliflozin, in a dose of 15 mg/kg/d, was administered from week 10 until euthanasia (week 16). By week 16, blood was drawn from the inferior vena cava of anesthetized rats to induce hemorrhagic shock and death. 24-hour urine collection using metabolic cages, and blood sampling were performed at weeks 1 (baseline), 4, 10, and 16. Blood samples were centrifuged at 3000 rpm at 4 ℃ for 10 min. The urine samples were centrifuged for 10 min at 2000 rpm. Plasma and urine supernatant samples were stored at − 80 ℃ for later experiment. The kidneys were weighed and cut longitudinally into two halves; one half was preserved in 4% paraformaldehyde and paraffin-embedded for histological analysis and the other half was used for single-cell RNA sequencing.

2.2. Plasma and urine analysis

Levels of plasma creatinine (Scr), urine creatinine, and urine microalbumin (n = 6–9 per group) were tested using commercially available enzyme-linked immunosorbent assays (Elabscience, Wuhan, China). Blood urea nitrogen (BUN) was determined quantitatively using automatic biochemistry analyzer (Hitachi High-Technologies, Tokyo, Japan). The urinary albumin-to-creatinine ratio (UACR) was calculated.

2.3. Kidney morphology

The harvested kidneys were cut into 4 μm thick sections and were stained with hematoxylin and eosin (H&E) and Masson's trichrome staining. The degree of glomerular and interstitial injury was determined by scoring inflammation, tubular dilatation, and tubular cast in ten randomly consecutive fields (25 ×25 μm) on 200x magnified H&E-stained images. The following criteria were used to evaluate H&E scores: 1 (≤ 10%), 2 (11–25%), 3 (26–45%), 4 (46–75%), and 5 (≥ 76%) [17]. The interstitial and glomerular fibrosis were estimated by Masson's trichrome staining at 200x magnification. Ten non-overlapping microscopic fields were captured. A random image subset was utilized to estimate the detection value for fibrotic regions (blue positive area) under each microscopic field using imageJ software. The percentages of fibrotic areas in each segment were then determined. Kidney morphology was judged by 2 blinded independent investigators.

2.4. Tissue dissection

Fresh kidney tissues were washed three times with balanced salt solution (HBSS), cut into 1–2 mm pieces, and digested for 15 min at 37 ℃ using GEXSCOPE tissue dissociation solution. After separating the

cells from cell debris with a 40-micron sterile strainer (Falcon), we centrifuged the filtered cells and resuspended the cell pellets in PBS (HyClone). The red blood cells were removed by adding GEXSCOPE Erythrocyte Lysis Buffer (Singleron) to the cell suspension. The cells were counted using TC20 Automated Cell Counter (Bio-Rad) to obtain a final cell suspension concentration of 1×10^5 cells/ml.

2.5. ScRNA-seq quantification and data analysis

Single cell suspensions with concentration of 1×10^5 cells/ml were loaded onto microfluidic apparatus. Following the Singleron GEXSCOPETM protocol, we constructed scRNA-seq libraries using GEXSCOPETM single cell RNA library kit (Singleron Biotechnologies). Individual libraries were diluted to 4 nM and pooled for sequencing on the Illumina Hiseq X platform with 150 bp paired-end reads. Raw fastq files were matched to the Ensembl Rnor_6.0 reference genome, followed by gene quantification performed by FeatureCounts. The data quality control, preprocessing, and dimensional reduction were performed by Seurat R package (V3.1.2). To obtain high-quality matrices, cells with < 200 or $>$ 3000 expressed genes, UMIs $< 30{,}000$, and the percentages of mitochondrial genes > 50 were eliminated. After data normalization using robust point matching (RPM), we selected the 2000 highly variable genes for principal component analysis (PCA). The top 20 dimensions were utilized in visualization and clustering. Cell clustering was done using FindClusters function with a resolution of 0.8, which resulted in 14 distinct cell clusters. To explore the heterogeneity in myeloid cell and T cell clusters, we used a resolution of 1.2 for the subclustering of myeloid and immune cells. The FindMarkers function with the default parameters (Benjamini-Hochberg adjusted *P* value < 0.05 in Wilcoxon rank sum test) was used to identify differentially expressed genes between cell clusters.

2.6. scRNA-seq trajectory analysis

To identify the distinct states of M2 macrophages and clarify the temporal differentiation trajectory between these cells, Monocle3 v0.1.3 was used to construct the pseudotime trajectory for M2 macrophages polarization. The cells were arranged along pseudotime trajectory. DifferentialGene Test function of Monocle3 were used to discover highly variable genes between different M2 macrophage states. Significant changes were defined as genes with an adjusted *P* value < 0.05 and were kept for further analysis. We used gene set variation analysis (GSVA), a non-parametric and unsupervised analytical approach for assessing the enrichment intensity of different pathways in samples, to characterize the enrichment of immunoinflammatory pathways in M2 macrophages at different stages.

2.7. Pathway enrichment analysis and gene regulatory network inference

We conducted kyoto encyclopedia of genes and genomes (KEGG) and gene ontology (GO) analyses using ClusterProfiler (3.10.1) R package. Enrichment of pathway and biological process was defined based on Benjamini-Hochberg adjusted *P* value < 0.05. To identify the variation of key transcription factors (TFs) during macrophage transformation, SCENIC, a robust R package for single-cell regulatory network inference and cell clustering, was applied to perform cis-regulatory analysis based on co-expression and DNA motif matrices. The process and description of SCENIC analysis were detailed at https://github.com/aertslab/SCENIC.

2.8. Cell interaction analysis

To evaluate the cellular connections between immune cells and macrophages, we inferred cell-cell communication networks using the CellPhoneDBv2.1.2 repository. CellPhoneDB, a python-based computational analysis tool, was used to calculate the score of ligand-receptor interactions and P value across the cell populations. The process and description of CellPhoneDB analysis were detailed at https://github.com/Teichlab/cellphonedb. First, we performed homologous gene conversion between human and rat. We then set the screening threshold of cells expressing receptors and ligands within each cluster to 0.1 and the iterations to 1000. Significant ligand-receptor pairs between cell types were defined as those with a P value < 0.05. NicheNet was used to assess the target genes of ligands-receptor pairs between M2 macrophages and T cell subpopulations. We set M2 macrophage and T cell suspopulations as receiver and sender cells, respectively. The detail of NicheNet analysis is available at https://github.com/saeyslab/nichenetr. Finally, we used ingenuity pathway analysis (IPA) to predict the correlation between genes (https://digitalinsights.qiagen.com/). Genes with significant changes between groups (adjusted $P < 0.05$ and $|\text{Log2FC}| > 0.58$) were input in the IPA software.

2.9. Statistical information

GraphPad Prism version 8.0 and SPSS 26.0 software were used for statistical analysis and graphic charting. For the statistical analysis of laboratory indicators, One-way ANOVA analysis and Kruskal-Wallis tests of variance were used to compare normally and non-normally distributed data, respectively. The differentially expressed genes analysis was performed using Wilcoxon rank sum test. FDR method was used to correct for multiple testing error.

3. Results

3.1. Kidney function and morphology

The flowchart of the study is illustrated in Fig. 1a. Blood pressure and body weight were not different among the groups (Fig. 1b). 5/6 Nx caused an increase ($P < 0.0001$) in blood urea nitrogen, serum creatinine, urine albumin-to-creatinine ratio, and empagliflozin treatment blunted this effect ($P < 0.0001$). (Fig. 1b). Tubular cast and glomerular injury scores were increased by 5/6 Nx and empagliflozin treatment improved it ($P < 0.001$). In addition, glomerular and tubulointerstitial fibrosis were higher in the 5/6 Nx group, and likewise empagliflozin treatment improved it ($P < 0.05$) (Fig. 1c, d).

3.2. Single-cell profiles of 5/6 Nx CKD

We randomly selected three kidney samples from each group to generate a scRNA-seq atlas. After data quality control, preprocessing, and dimensional reduction, we separated 89420 cells into 14 distinct cell clusters. Supplementary Figure 1 depicts the quality control metrics for each sample. Based on the gene expression markers (Supplementary Table 1), we identify clusters representing T cells (marker: *CD3G*), myeloid cells (*LYZ2*), proximal tubule cells (*LRP2*), distal tubule cells (*SLC12A3*), loop of Henle (*SLC12A1*), collecting duct principal cells (*AQP2*), collecting duct intercalated cells (*FOXIL*), ureteric epithelium (*UPK3A*), endothelial cells (*CDH5*), fibrocytes (*DCN*), mesangial cells (*ITGA8*), smooth muscle cells (*TAGLN*), pericytes (*RGS5*), and proliferating cells (*TOP2A*) (Fig. 2a-c, Supplementary Figure 2a). The matrix of differential expression genes for each cell type is accessible in Supplementary Table 2. The percentage of different cell types revealed that just a few myeloid cells were detected in the Sham group, while myeloid cells were dramatically increased in the 5/6Nx group and significantly decreased following empagliflozin therapy (Fig. 2d, Supplementary Figure 2b). We discovered that changes in the percentage of fibrocytes were proportional to myeloid cells (Supplementary Figure 2b). Additionally, the functional enrichment analysis showed an active biological process of filament formation in myeloid cells, suggesting a close link between myeloid cells and fibrocytes (Supplementary Figure 3a). To obtain further insight into the role of myeloid cells in the 5/6Nx CKD, we then focused our research efforts on analyzing the cellular heterogeneity

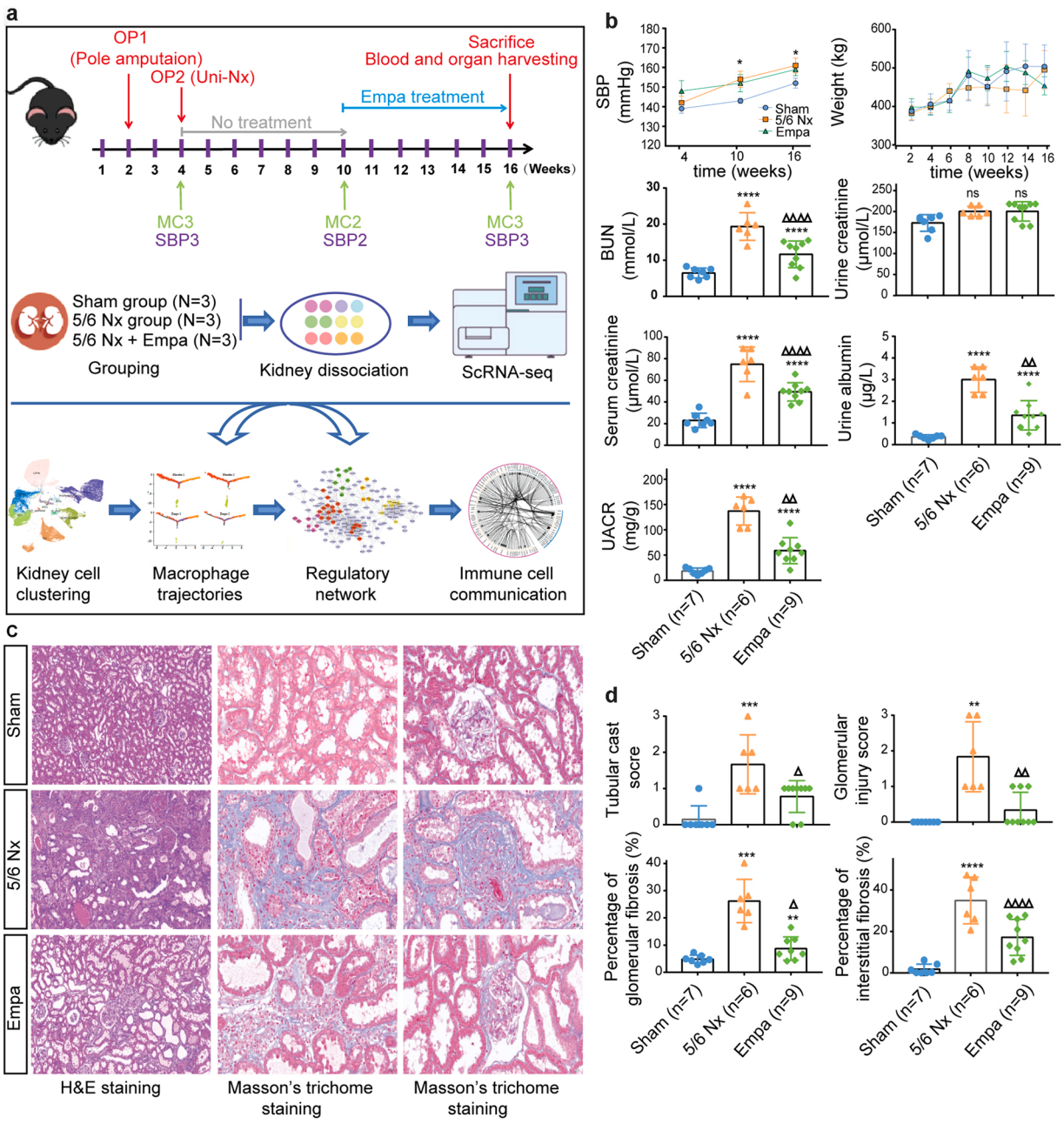

Fig. 1. The effects of empagliflozin on renal function and morphology in 5/6 nephrectomy CKD. (a) Schematic of the experimental design and analyses. (b) Histograms showing changes in kidney injury indicators before and after empagliflozin therapy. (c) H&E and Masson's trichome staining (x 200) depicting the histological alterations in kidney tissues in each group. (d) Histograms showing renal morphology scores based on 10 randomly consecutive fields in each section, as well as the percentages of interstitial and glomerular fibrosis. The symbols * and Δ represent statistical comparisons with the Sham and 5/6 Nx groups, respectively. * /Δ $P < 0.05$; **/ΔΔ $P < 0.01$; * ** /ΔΔΔ $P < 0.001$; ****/ΔΔΔΔ $P < 0.0001$. Abbreviations: ScRNA-seq, single-cell RNA sequencing; BUN, blood urea nitrogen; UACR, urinary albumin-to-creatinine ratio; 5/6 Nx, 5/6 nephrectomy; Empa, empagliflozin; MC, metabolic cage; OP1, operation 1 (amputation of the poles of the left kidney); OP2, operation 2 (excision of the right kidney); SBP, systolic blood pressure measurement; Uni-Nx, uninephrectomy of the right kidney.

between myeloid cell subsets.

3.3. Specific changes in M2 macrophage before and after empagliflozin treatment

After subclustering of the myeloid cells, we identified six subpopulations of myeloid cells, including M1 macrophage (*IL1B*), M2 macrophage (*C1QB*), monocytes (*SELL*) and three dendritic cell subsets (Fig. 3a, c and Supplementary Figure 3b). Supplementary Table 3 shows the gene expression matrix for each myeloid cell subset. We found the proportion of monocytes and M1 macrophages was significantly reduced, while that of M2 macrophage was strikingly increased in the 5/6Nx group, indicating that a majority of monocytes and/or M1 macrophage might have converted to M2 macrophage. Interestingly, M2 macrophage showed a significantly lower proportion after empagliflozin treatment, with subsequentially increased number of M1 macrophages (Fig. 3c, Supplementary Figure 3c, d). In addition to interfering with M2 macrophage production, empagliflozin decreased gene transcription levels in M2 macrophages (Fig. 3d), particularly in M2 macrophage polarization genes (*GPNMB, LGALS3*, *PRDX5*, and *CTSB*) [18,19] and fibrosis-promoting genes (*IGF1* and *TREM2*) [20,21] (Fig. 3e). Those genes that were down-regulated by empagliflozin primarily reflected

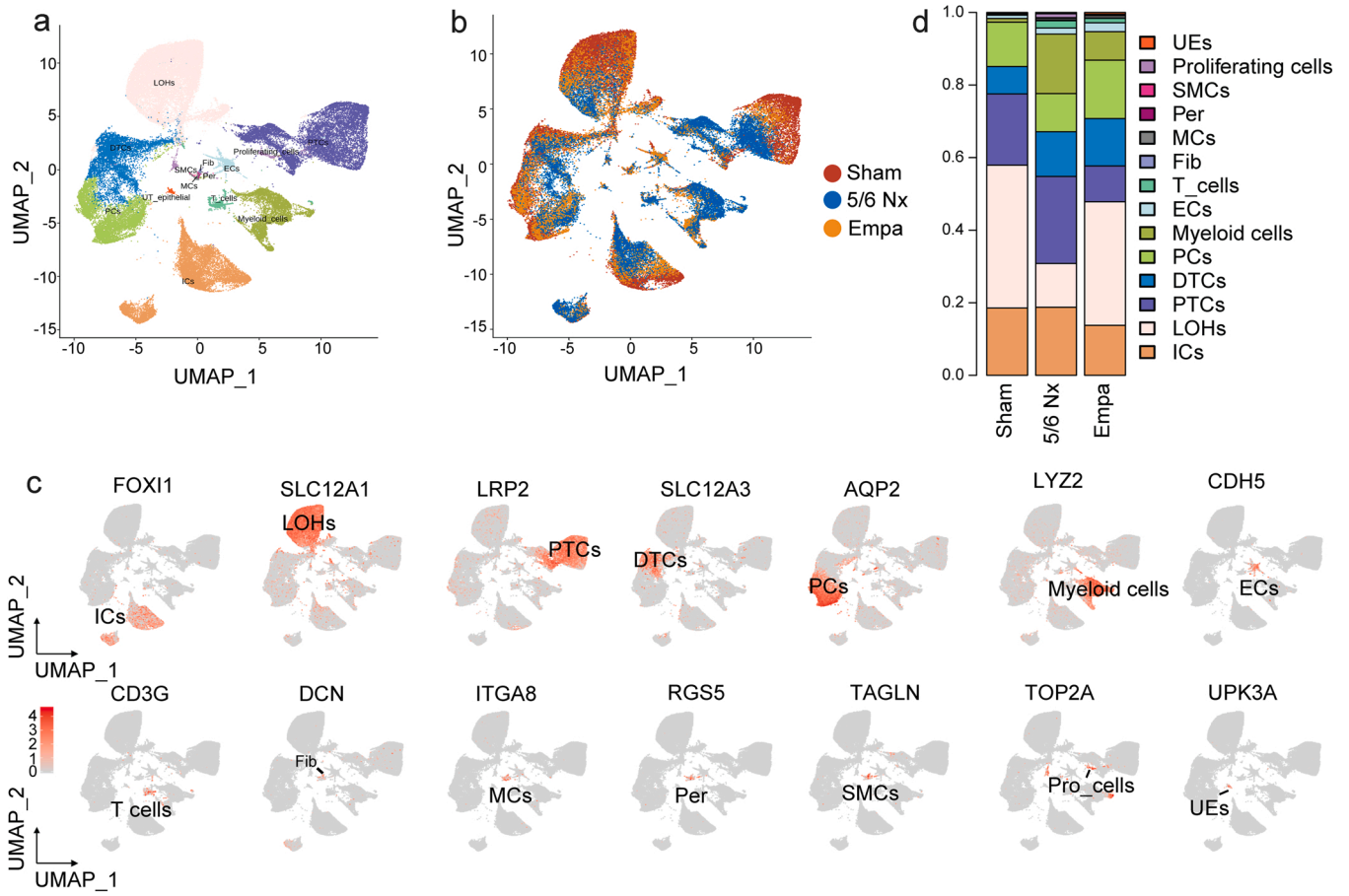

Fig. 2. Single-cell profiles identified major cell types in the 5/6 nephrectomy CKD. (a) Dimensionality reduction and clustering of 89420 cells. (b) UMAP embeddings of scRNA-seq data colored by group batches. (c) Based on the expression of representive marker genes, clusters were annotated into T cells, myeloid cells, proximal tubule cells (PTCs), distal tubule cells (DTCs), loop of Henle cells (LOHs), collecting duct principal cells (PCs), collecting duct intercalated cells (ICs), ureteric epithelium cells (UEs), endothelial cells (ECs), fibrocytes (Fib), mesangial cells (MCs), smooth muscle cells (SMCs), pericytes (Per), and proliferating cells (Pro_cells). (d) Stacked bar graphs depicting the alterations in the percentage of different cell subsets between groups.

diminished immunoreactivity, oxidative phosphorylation, and ATP biosynthetic process in M2 macrophages (Fig. 3f, Supplementary Table 4), which have been reported to be important processes affecting M2 macrophage polarization [22], supporting the role of empagliflozin in inhibiting M2 macrophage polarization.

Given that M2 macrophages execute various roles in different states, we identified five different developmental stages of M2 macrophages using trajectory analysis (Fig. 3g). M2 macrophages in state 1 strongly expressed division-related genes, referring to M2 macrophages in the early differentiation stage. M2 macrophages in state 3 were predominantly involved in the immunological response, representing a group of functioning M2 macrophages that conducted immune function (Fig. 3 h, Supplementary Table 5, 6). We found upregulation of M2-polarized phenotypic marker genes *CD206* and *CD68* in M2 macrophages in states 4 and 5 (Fig. 3i). *CD206*$^{+}$*CD68*$^{+}$ M2 macrophages have been proven to have the potential to convert into fibrocytes [23]. Notably, we only discovered overexpression of fibrosis-related genes and active biological process of fibroblast proliferation in M2 macrophages in state 5 but not in M2 macrophages in state 4 (Fig. 3h), suggesting that the phenotype of M2 macrophages in state 5 was the primary cause for fibrogenesis in CKD. Importantly, empagliflozin remarkably inhibited the production of M2 macrophages in states 3 and 5 (Fig. 3g). For this reason, we set out to unravel the mechanism underlying the pro-fibrotic polarization process of *CD206*$^{+}$*CD68*$^{+}$ M2 macrophages from state 1 to state 3 to state 5, as well as to characterize the targeted effects of empagliflozin on M2 macrophage polarization.

3.4. Regulatory mechanisms for *CD206*$^{+}$*CD68*$^{+}$ M2 macrophage polarization

We used gene set variation analysis to identify the enriched pathways of M2 macrophage in different stages. The results showed that lysosome, mitophagy, and mTOR pathways were gradually enhanced during the polarization process of *CD206*$^{+}$*CD68*$^{+}$ M2 macrophages. Most importantly, the degrees of enrichment for the aforementioned pathways were attenuated after empagliflozin therapy (Fig. 4a). Fig. 4b depicted the changes in gene expression in the relevant pathways over pseudotime. We noticed that these genes increased over time in the 5/6Nx group, while empagliflozin significantly suppressed their expression levels, especially in *CD206*$^{+}$*CD68*$^{+}$ M2 macrophages. To investigate changes in transcription factors (TFs) during M2 macrophage polarization and their putative target genes, we used SCENIC to evaluate TF regulon activity in each M2 macrophage state and construct TF-centered gene co-expression networks. First, SCENIC successfully conducted cell-state identification, which were in keeping with the results of the trajectory analysis (Supplementary Figure 4). Also, SCENIC further revealed robust enrichment in *IRF9*, *CREB5*, *NFIC*, *THAP1*, *RFX5*, *BRCA1*, *SETDB1*, *HSF1*, and *RELB* regulon activity in M2 macrophages in state 1, *NFATC3*, *ETS1*, *BMYC*, *MYC*, *NFYA*, *KDM5B*, *FOXIL*, *BACH*, *FOXP2*, and *EGR3* in M2 macrophages in state 3, and *MEIS*, *FOSB*, *FOS*, *EGR1*, *TFEC*, *CEBPD*, *MXD4*, *ATF4*, and *SMAD5* in M2 macrophages in state 5, respectively (Fig. 4c). Finally, SCENIC inferred target genes of each TF in each regulon and established the regulon-TF-gene modules (Supplementary Table 7). Based on these co-expression matrix, we next

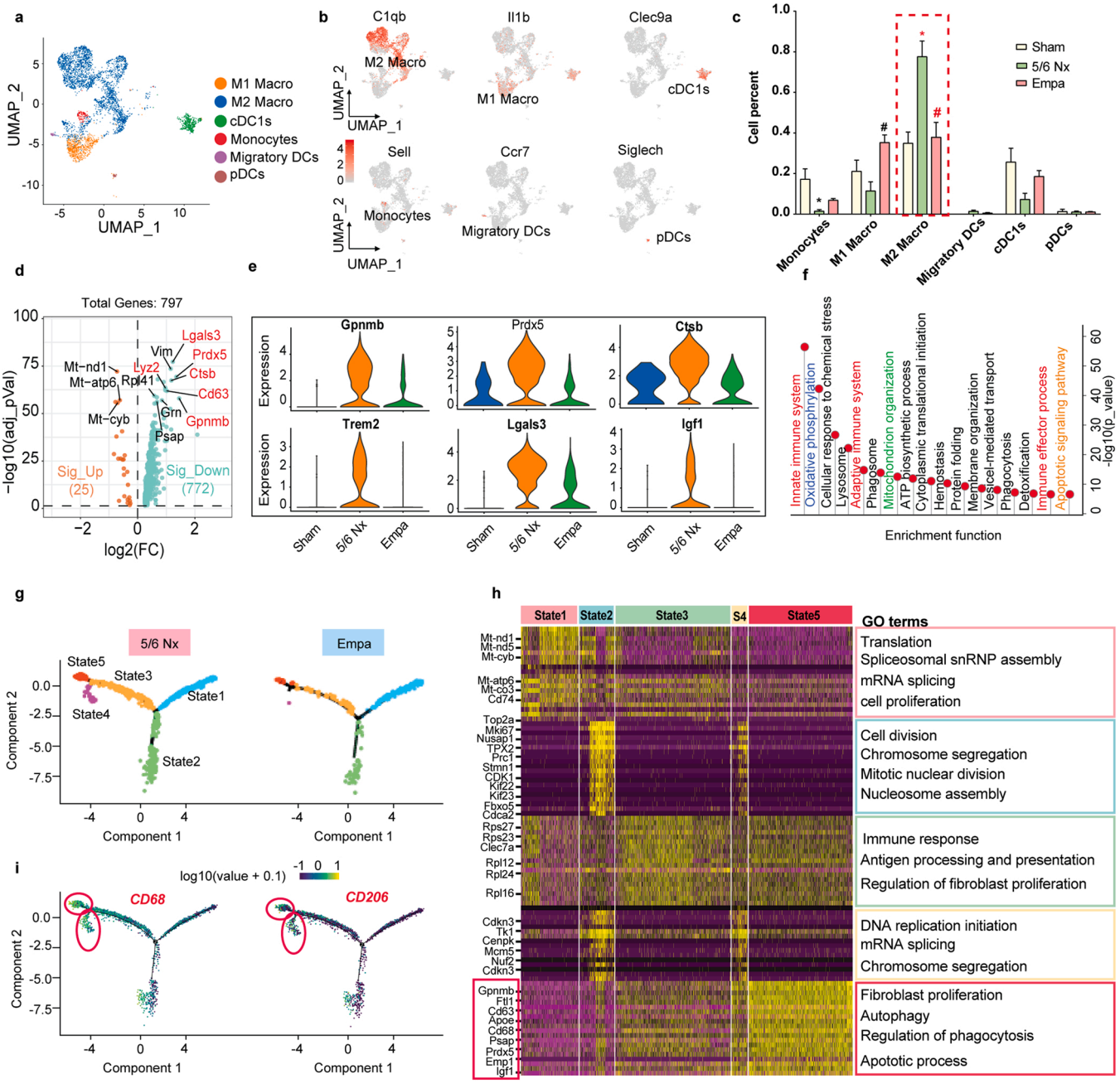

Fig. 3. Specific effects of empagliflozin on M2 macrophage in 5/6 nephrectomy rat kidney. (a) UMAP plot visualizing subclustering of rat kidney myeloid cells. (b) Dotplot showing representative marker gene expression levels in the myeloid cell subpopulations. Subclusters were annotated into M2 macrophages (M2 Macro), M1 macrophages (M1 Macro), monocytes, migratory dendritic cells (Migratory DCs), conventional type I dendritic cells (cDC1s), plasmacytoid dendritic cells (pDCs). (c) Bar graphs depicting the alterations in the percentage of myeloid cell subpopulations between groups. * and # represent statiscia statistical comparison with the Sham and 5/6 Nx groups, respectively. * and # represent a P value < 0.05. (d) Volcano plot showing the differentially expressed genes in M2 macrophages between the 5/6 Nx and Empa groups (5/6 Nx vs. Empa). A total of 797 altered genes were identified between groups, with 772 down-regulated and 25 up-regulated genes following empagliflozin therapy. Fold change > 2 or < 0.5 and adjusted P < 0.05 were used as screening criterion. (e) Violin plots showing the differential expression of macrophage polarization genes (*GPNMB*, *LGALS3*, *PRDX5*, and *CTSB*) and fibrosis-promoting genes (*IGF1* and *TREM2*) across groups. (f) Significant differences in biological processes between the 5/6 Nx and Empa groups. The strength of the P value for each term was shown by the length of the lines under that phrase. (g) Internal differentiation trajectory of M2 macrophages, as inferred by Monocle3. Each time branch represents an M2 macrophage state. Cells are colored by pseudotime. (h) Heatmap depicting the differential gene expression changes in each state of M2 macrophage. Genes surrounded by a red frame highlight the upward trend of macrophage polarization genes and fibrosis-promoting genes from state1 to state5. Biological processes of M2 macrophage in each state were identified based on the representative genes. Representative genes in each M2 macrophage state were filtered by fold change > 2 or < 0.5 and adjusted P < 0.05 in comparison to the remaining M2 macrophage states. (i) Levels of CD68 and CD206 expression in M2 macrophages differentiation trajectory.

performed functional enrichment analysis using downstream target genes that were regulated by the key TFs in each regulon. Interestingly, *CD206*$^{+}$*CD68*$^{+}$ M2 macrophage-specific TFs were shown to be involved in the gene regulation of lysosome, mitophagy, and mTOR pathways, revealing a TF-regulatory network for *CD206*$^{+}$*CD68*$^{+}$ M2 macrophage polarization (Fig. 4d, e). The impact of empagliflozin on these TFs was next investigated and the results showed that empagliflozin had inhibitory effects on *MEIS3*, *TFEC*, *CEBPD*, *EGR1*, *ATF4*, and *MXD4* expression

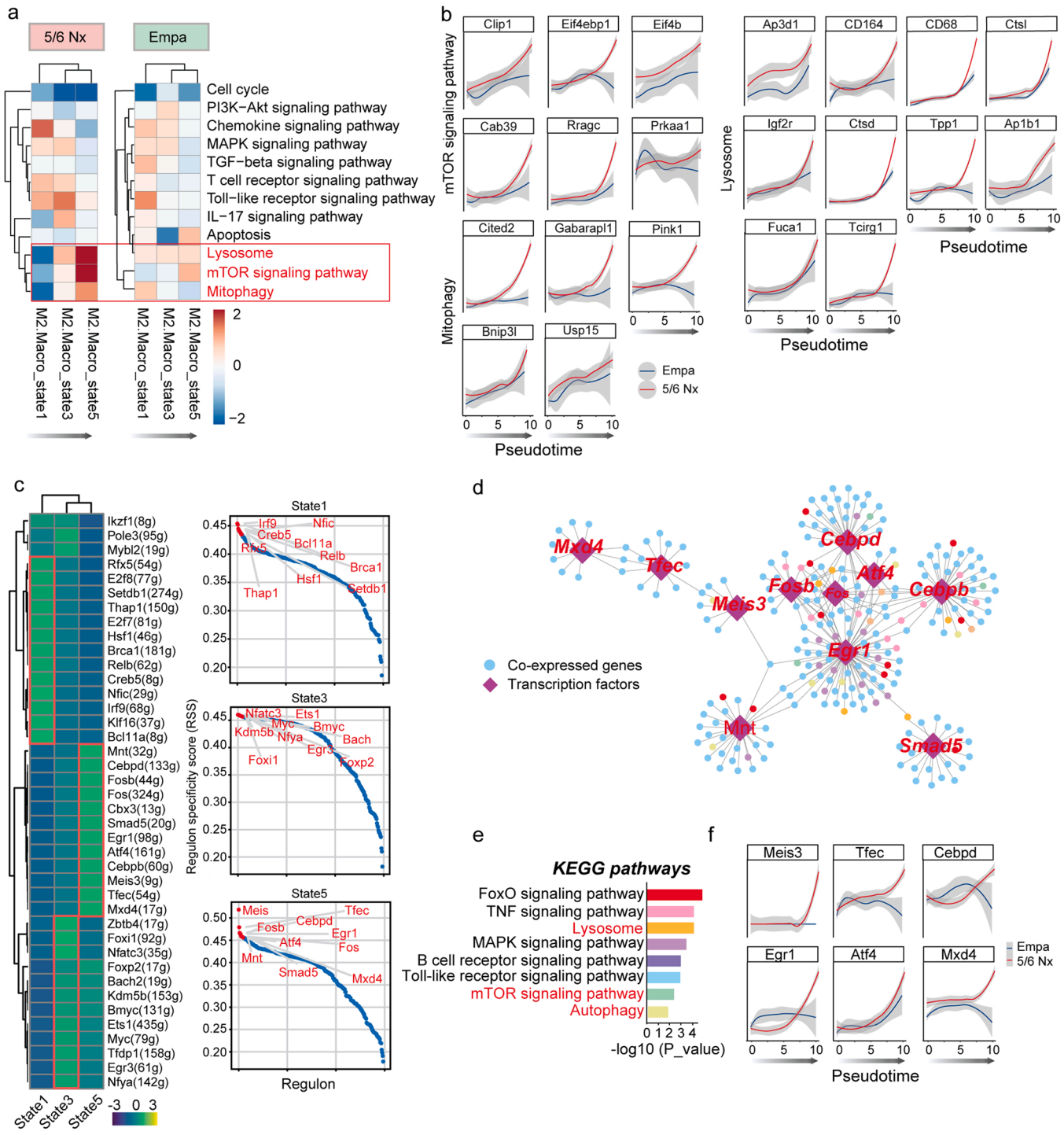

Fig. 4. Effects of empagliflozine on the regulatory mechanisms of CD206^{+}CD68^{+} M2 macrophage polarization. (a) Heatmap depicting alterations in pathway activities scored by GSVA during CD206^{+}CD68^{+} M2 macrophage polarization. GSVA enrichment score for each pathway was denoted by different colors. (b) Changes in Pseudotime-dependent gene expression. The red lines represent the dynamic changes of the key genes related to lysosome, mitophagy, and mTOR signaling pathways during CD206^{+}CD68^{+} M2 macrophage polarization (form state1 to state3 to state5) in the 5/6 nephrectomy group, while blue lines indicate changes in these genes after empagliflozine intervention. The error bars represent the 95 % confidence intervals for fitting local polynomial regressions. (c) Left panel: z-score heatmap of the top TFs in each state of M2 macrophage. Right panel: specific regulons of M2 macrophage in different states, as inferred by SCENIC algorithm. (d) The regulatory network of the TFs regulating CD206^{+}CD68^{+} M2 macrophage polarization. The co-expression genes for each TF are listed in Supplementary Table 6. Rhombus represent TFs and circles denote target genes. The colors of the circles represent the genes related to corresponding pathways shown in (e). Significant KEGG enrichment pathways on co-expression genes of these TFs are presented in (e). (f) Changes in pseudotime-dependent TFs expression before (red lines) and after (blue lines) empagliflozine therapy. Abbreviations: GSVA, gene set variation analysis; TF, transcription factor; KEGG, Kyoto Encyclopedia of Genes and Genomes.

(Fig. 4 f).

3.5. Cellular communication between T cell subpopulation and M2 macrophage

The function of T-cell cytokines in macrophage activation and polarization has gained credence. After identifying four T cell subpopulations, including CD8 + effector T cells (marker: *NKG7*), T helper cells 17 (Th17; marker: *CCR6*), regulatory T cells (Treg; marker: *TNFRSF4*), and follicular helper T cells (Tfh; marker: *CXCR6*) (Fig. 5a, b), we then systematically inferred cell-cell communication networks using the CellPhoneDB R package. Based on our scRNA-seq dataset, we found a greater number of cell-cell interaction pairs between M2 macrophage and T cell subpopulations in 5/6Nx CKD (Fig. 5c). Interestingly, empagliflozin effectively decreased the number of these present interaction pairs, suggesting that empagliflozin interfered with cellular communication between M2 macrophage and T cell subpopulations. The top receptor-ligand pairs revealed that empagliflozin inhibited the levels of *CSF2-CSF1R*, *COPA-P2RY6*, *TNFSF14-LTBR*, *TNFRSF1B-GRN*, and *CCL5-CCR1*, whereas activating *LAMP1-FAM3C* and *SPP1-CD44* expression (Fig. 5d). Herein, we further performed an in-depth analysis of downstream genes of *CCL5-CCR1* throughout the process of $CD8^+$ effector T cell - to - M2 macrophage communication, since the *CCL5-CCR1* gene knockout has been shown to exert strong antifibrotic effects in glomerulosclerotic mice [24]. However, we cannot rule out the possibility that other top receptor-ligand pairs have potential effects on kidney fibrosis as well. But to the best of our knowledge, this was not described so far for these gene pairs. NicheNet provides a robust database as well as a statistically-based strategy for predicting the downstream target genes of receptor-ligand interactions. We first estimated the activity of the ligands in the 5/6 Nx group based on the scRNA-seq dataset and ranked the top ligands. *CCL5* was identified as one of the top ligands, and the major cell type transmitting these signals was $CD8^+$ effector T cells (Supplementary Figure 5), which was consistent with the findings of CellPhone analysis. Empagliflozin, as expected, could decrease *CCL5* ligand activity (Fig. 5e). We then inferred the active target genes of the top ligands to establish a ligand-target linkage. Our findings suggested that *ATF3*, *CCL2*, *CEBPB*, *FOS*, *DUSP1*, *ITGB2*, *JUN*, *LMNA*, *TRIB1*, *UBC*, *ZFP36L1*, *FN1*, and *EGR1* were the mainly predicted target genes of *CCL*5 (Fig. 5f), of which *ATF3*, *FOS*, *TRIB1* and *EGR1* were crucial genes affecting macrophage polarization. Meanwhile, we also identified that *CCR1* and *CCR5* were the primary receptors for *CCL5* signaling (Fig. 5g). Most importantly, these receptors (*CCR1* and *CCR5*) and target genes of *CCL5* showed uptrend during the process of $CD206^+CD68^+$ M2 macrophage polarization and were partly attenuated after empagliflozin treatment (Fig. 5h), suggesting that empagliflozin may suppress $CD206^+CD68^+$ M2 macrophage polarization by regulating *CCL5-CCR1* downstream gene expression.

Considering the complex intracellular genes management network, we speculated that downstream target genes of *CCL5-CCR1* may interact with genes on the mTOR-mitophagy pathway and synergistically influence M2 macrophage polarization. Therefore, we used ingenuity pathway analysis to infer the interplay between these key genes and ultimately constructed a complete regulatory network for M2 macrophage polarization. As expected, these genes, which were progressively elevated during M2 macrophage polarization, showed internal regulatory connections (Supplementary Figure 6a). Importantly, empagliflozin could effectively suppress the expression of these genes, indicating that empagliflozin might inhibit M2 macrophage polarization by interfering with *CCL5-CCR1* signaling, mTOR-mitophagy and lysosome pathways (Supplementary Figure 6b). These findings provided potential strategies for reversing or inhibiting the fibrosis development during CKD.

4. Discussion

SGLT2 inhibitors were originally developed and approved for the treatment of type 2 diabetes. However, safety studies required by regulatory authorities surprisingly showed that this class of agents is also very effective in slowing down the progression of chronic renal failure in patients with guideline-based therapy for chronic renal failure, independent of the blood glucose lowering effect. Although this class of compounds has such excellent clinical properties, the underlying mechanisms are poorly understood to date. The aim of our study was first to demonstrate that SGLT2 blockade in a non-diabetic CKD model can decrease urinary albumin excretion, slow down deterioration of GFR and fibrotic renal remodeling even after establishment of CKD. In this respect, the study design we chose differs from many animal studies performed so far [13,25,26]. Usually, the effects of SGLT2 inhibitors were investigated immediately after experimental induction of chronic renal failure and not, as in our study, when renal failure is already established. Our experimental study design is therefore much closer to the clinical situation in which the beneficial effects of SGLT2 inhibition on chronic renal failure has been described. We investigated possible mechanisms of late treatment with an SGLT2 inhibitor by single cell RNA sequencing, a novel technology allowing deep insights into underlying pathways. Our findings highlighted that empagliflozin could prevent the polarization of pro-fibrotic $CD206^+CD68^+$ M2 macrophage by targeting mTOR and mitophagy pathways and attenuating inflammatory signals from $CD8^+$ effector T cells, thereby attenuating renal fibrosis in 5/6 nephrectomiced rats with established CKD.

Endothelial-to-mesenchymal transition (EndMT) and macrophage-to-myofibroblast transition (MMT) is increasingly recognized as pathways leading to renal failure [23,27]. Indeed, the injured kidney undergoes two distinct phases: the acute inflammation phase and the resolution phase [23]. In the early stage of renal damage, bone-marrow-derived monocytes infiltrate into the kidney and differentiate into pro-inflammatory M1 macrophages (CD206- macrophages) in response to tissue injury [28,29], while the resolution phase is characterized by the conversion of pro-inflammatory M1 macrophages to anti-inflammatory M2 macrophages ($CD206^+$ macrophages) that are involved in immunosuppression and matrix remodeling [23,30]. However, it is important to note that $CD206^+$ M2 macrophages can further differentiate into αSMA^+ myofibroblasts via TGFβ1-Smad3 signaling [31], thereby promoting interstitial fibrosis [32,33]. Recent studies have elucidated the role of SGLT2 inhibitors in macrophage plasticity. In some inflammatory models, such as diet-induced obese and LPS-stimulated macrophage models, empagliflozin reduced pro-inflammatory M1 macrophage accumulation, while inducing the proliferation of anti-inflammatory M2 macrophages, thereby attenuating tissue inflammation [34,35]. The anti-inflammatory effects of empagliflozin were mainly mediated through the downregulation of *IKK/NF-κB*, *MKK7/JNK*, and *JAK2/STAT1* pathways in M1 macrophages [35]. Notably, one study showed that dapagliflozin could attenuate cardiac fibrosis by promoting M2 macrophage polarization in the early stage of infarcted rat hearts [36].

Our study, however, differs from previous work in several ways. First, we focused on the renal characteristics in the later stage of tissue repair where treatment was started only after CKD was established (see study design in Fig. 1), rather than the acute inflammation phase. We observed a massive accumulation of M2 macrophages and fibroblasts. Since we utilized the unique advantages of scRNA-seq to identify different stages of M2 macrophages, we were able to uncover the complexity of macrophage subpopulations in the progression of CKD like other already showed it for atherosclerosis and cancer [37,38]. We successfully detected five M2 macrophages stages. Trajectory analysis revealed that the polarization of M2 macrophages from state 1 ($CD206^-CD68^-$ M2 macrophages) to finally state 5 ($CD206^+CD68^+$ M2 macrophages) was the main pro-fibrotic process, as $CD206^+CD68^+$ M2 macrophages highly expressed fibrosis-promoting genes and had the potential to convert into fibrocytes [31–33]. Empagliflozin remarkably inhibited the expression levels of fibrosis-promoting genes (*IGF1* and *TREM2*) and polarization-associated genes (*GPNMB, LGALS3*, *PRDX5*,

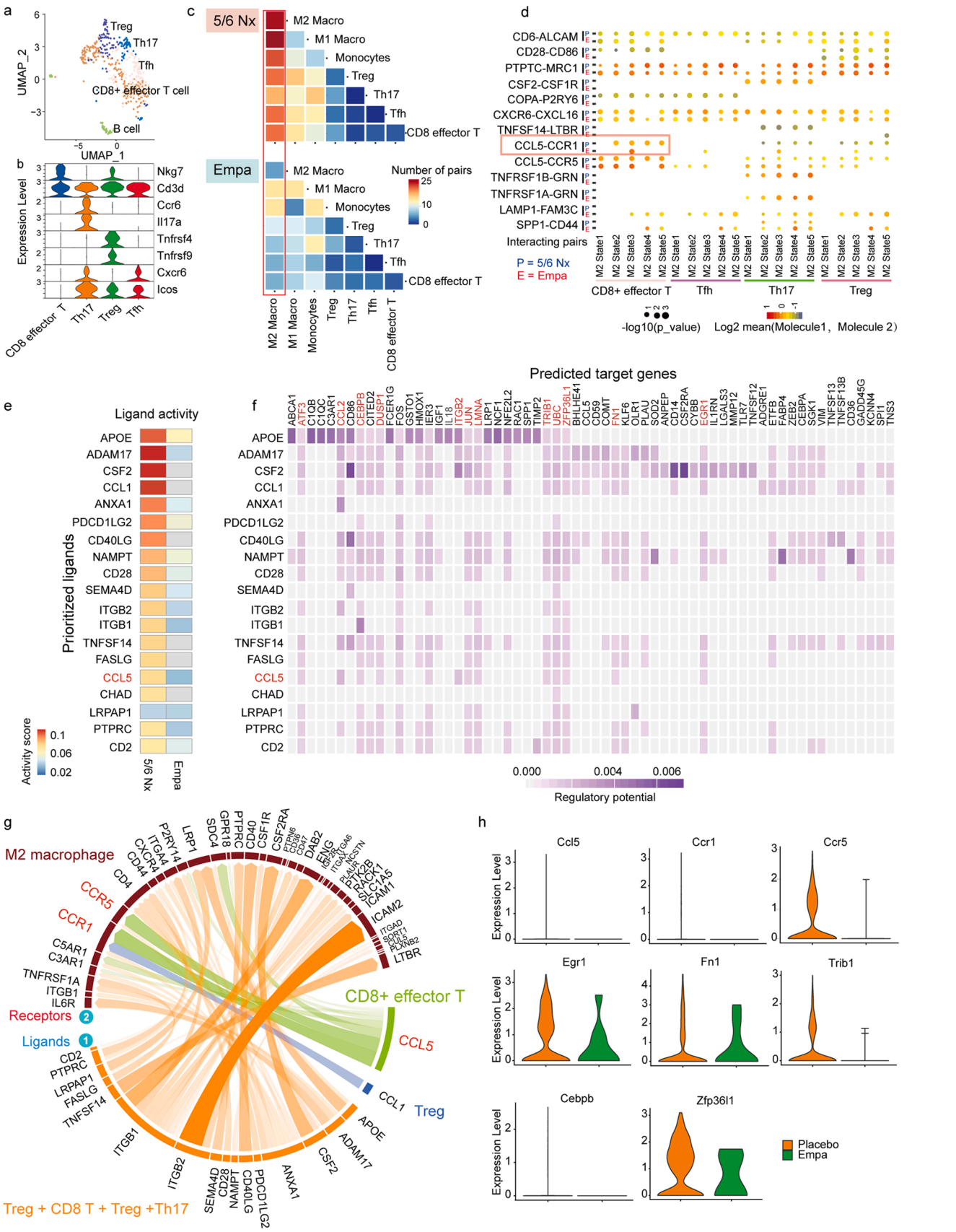

(caption on next page)

Fig. 5. Inhibitory effects of empagliflozin on cellular communication between T cell subpopulation and M2 macrophages. (a) UMAP plot visualizing subclustering of rat kidney immune cells. (b) Violin plots showing cell type-specific gene expression in T cell subpopulations. (c) Heatmap depicting the number of ligand-receptor pairs between each T cell subset and M2 macrophages, as inferred by CellPhone algorithm. The progression from blue to red indicates a gradual increase in the number of pairs. (d) Bubble plots showing the top ligand-receptor pairs with significant P value < 0.05 between T cell subpopulations and M2 macrophages before and after empagliflozin intervention. The size of the dots corresponds to the relevant P values of the permutation test with 1000 permutations. Color scale denotes the mean values of the ligand-receptor pairs, where mean value is calculated by the total mean of the average expression of ligands in a cluster and the average expression of receptors in the interacting cell cluster. (e) Schematic illustration depicting the top-ranked ligands detected by NicheNet. The progression from blue to red denotes a gradual increase in score of ligand activity. (f) Heatmap showing the regulatory potential of these prioritized ligands expressed in T cell subpopulations for the predicted target genes expressed in M2 macrophages. (g) Circos plot showing the key receptors for these prioritized ligands acting on M2 macrophages. The size of the line represents the strength of the ligand-receptor activity. Green and blue lines denotes the ligand signal specially derived from CD8 + effector T cells and regulatory cells, respectively. (h) Violin plots showing the differential expression of *CCL5* target genes among groups.

and *CTSB*) in $CD206^{+}CD68^{+}$ M2 macrophages. We suggest that this represents a novel key anti-fibrotic mechanism of empagliflozin in established CKD. It is worth noting that M2 macrophages can be subdivided into M2a, M2b and M2c [23]. However, due to the weak capacity of the single-cell sequencing technology to identify M2 macrophage subpopulations, we are unable to determine which type of M2 macrophages are predominantly inhibited by Empagliflozin.

Furthermore, our findings suggested that the inhibitory effect of empagliflozin on $CD206^{+}CD68^{+}$ M2 macrophages polarization was mainly achieved by controlling mitophagy and mTOR pathways. The relevance between mitophagy and macrophage phenotypic transformation in the injured kidney is well established. It has been described that mitophagy activation remarkably stimulated the conversion of M1 macrophages to the M2 phenotype. Conversely, mitophagy inhibition significantly promoted macrophages to convert into the M1 phenotype [39,40]. In line with previous reports, our study showed an increasing mitophagy activity during polarization from $CD206^{-}CD68^{-}$ M2 macrophages to $CD206^{+}CD68^{+}$ M2 phenotype in 5/6 nephrectomy rat. Importantly, empagliflozin effectively decreased the expression levels of mitophagy-related genes (*PINK1*, *CITED2*, *GABARAPL2*, *BNIP3L*, and *USP15*) and lysosome-related genes (*CD68*, *CD164*, *FUCA1*, *IGF2R*, *TCIRG1*, *CTSD*, *CTSF*, *AP1B1*, *AP3D1,* and *TPP1*). This fits well with an earlier study. During ischemia-induced autophagy activation, empagliflozin directly suppressed Na^{+}/H^{+} exchanger 1 activity in cardiomyocytes to control excessive autophagy [41]. However, the impact of empagliflozin on mitophagy remains controversial, as some studies have shown stimulatory actions of empagliflozin on mitophagy [42,43]. In addition to the mitophagy pathway, the mTOR pathway is also critical for M2 macrophages polarization. Our findings showed an increase in some mTOR-related genes during the $CD206^{+}CD68^{+}$ M2 phenotype polarization. Previous studies showed that BMP-7 treatment polarized monocytes into M2 phenotype by targeting the PI3K-mTOR pathway [44]. Metformin could significantly promote M2 phenotype polarization by regulating the AMPK/mTOR pathway, thereby accelerating fibrogenesis [45]. The mTOR signaling pathway was also considered one of the main targets for SGLT2 treatment in some diseases such as Alzheimer's disease, diabetic nephropathy, and cancer [46–48]. We, herein, also found a suppressive effect of empagliflozin on the expression levels of some mTOR-related genes (*CLIP1*, *EIF4EBP1*, *EIF4B*, *CAB39*, *RRRAGC*, *PRKAA1*), suggesting that regulating mTOR could reduce M2 macrophages polarization. Notably, the mTOR pathway and mitophagy were tightly linked, as the mTOR pathway could effectively affect mitophagy [49,50]. Ingenuity pathway analysis based on our scRNA data also revealed a close interplay between mTOR and mitophagy-related genes (Supplementary Figure 6).

Our study also has limitations. We deliberately chose a CKD model, where chronic kidney disease is already established, to bring our study closer to the clinical situation. However, we did not examine the effects of empagliflozin immediately after starting therapy, but only at the end of the study. Thus, it remains to be shown whether the effect we observed on macrophage polarization is also detectable immediately after initiation of therapy. It would be equally important to know whether such mechanisms are also found in diabetic CKD. Our findings are based on observations of cell-type specific alterations of gene expression patterns. In particular, the exact molecular pathway how Empaglifloci targets immune cells needs to be figured out in further studies. Blood pressure in the control group was pretty high, because of somewhat noise recronstructions in the animal dacility while measuring blood pressure. However, blood pressure was clearly elevated in the placebo treated animal. Finally, it must be shown whether our findings can also be demonstrated with other SGLT2 blockers.

The beneficial effects of empagliflozin on kidney function and morphology in 5/6 nephrectomyiced rats with established CKD are at least partially due to an inhibition of $CD206^{+}CD68^{+}$ M2 macrophage polarization by targeting mTOR and mitophagy pathways and attenuating inflammatory signals from $CD8^{+}$ effector T cells. Additional studies are needed to investigate whether these effects are also detectable in diabetic CKD models as well as in humans with CKD treated with empagliflozin.

Authors' Contributions

Berthold Hocher designed the study, wrote and corrected the manuscript. Yongping Lu, Hongwei Wu and Ting Zhu perform data analysis and wrote the manuscript. Xitong Li, Zeyu Zhang, Xiaohua Wang, Jiao Zuo, Ahmed A Hasan, Christoph Reichetzeder, Denis Delic, Benito Yard, Thomas Klein, and Bernhard K. Krämer did laboratory analysis, analyzed data and corrected the manuscript. Lianghong Yin, Zhihua Zheng and Berthold Hocher prepared grant applications for this project.

Conflict of interest statement

The authors declare no competing interests.

Data Availability

Data will be made available on request. The data supporting the findings of this study are available in Additional files and from the corresponding author (berthold.hocher@medma.uni-heidelberg.de).

Acknowledgements

This work was supported by grants from Boehringer Ingelheim to Dr. Hocher, the National Natural Science Foundation of China (Grant No. 8210032527), GuangDong Basic and Applied Basic Research Foundation (Grant No. 2020A1515111209), and Young Innovative Talents Project of General Colleges and Universities in Guangdong Province (Grant No. 2018KQNCX010) and the China Scholarship Council (CSC) to Yongping Lu and Jiao Zuo supporting their PhD projects in Dr. Hocher`s team at the University of Heidelberg, Germany.

Appendix A. Supporting information

Supplementary data associated with this article can be found in the online version at doi:10.1016/j.biopha.2022.113947.

References

[1] K.R. Tuttle, F.C. Brosius, M.A. Cavender, et al., SGLT2 Inhibition for CKD and cardiovascular Ddisease in type 2 diabetes: report of a scientific workshop sponsored by the national kidney foundation, Diabetes 70 (1) (2021) 1–16.

[2] C. Wanner, S.E. Inzucchi, J.M. Lachin, et al., Empagliflozin and progression of kidney disease in type 2 diabetes, New Engl. J. Med. 375 (4) (2016) 323–334.

[3] B. Neal, V. Perkovic, K.W. Mahaffey, et al., Canagliflozin and cardiovascular and renal events in type 2 diabetes, New Engl. J. Med. 377 (7) (2017) 644–657.

[4] S.D. Wiviott, I. Raz, M.P. Bonaca, et al., Dapagliflozin and cardiovascular outcomes in type 2 diabetes, New Engl. J. Med. 380 (4) (2019) 347–357.

[5] V. Perkovic, M.J. Jardine, B. Neal, et al., Canagliflozin and renal outcomes in type 2 diabetes and nephropathy, New Engl. J. Med. 380 (24) (2019) 2295–2306.

[6] D.A. Molony, F.I. LeMaistre, In CKD, dapagliflozin reduced a composite of eGFR decline, end-stage kidney disease, or CV or renal mortality, Ann. Intern. Med. 174 (2) (2021) JC20.

[7] A. Shabaka, C. Cases-Corona, G. Fernandez-Juarez, Therapeutic insights in chronic kidney disease progression, Front. Med. (2021) 23.

[8] P. Fioretto, A. Zambon, M. Rossato, et al., SGLT2 inhibitors and the diabetic kidney, Diabetes Care 39 (2016) 165–171.

[9] S.C. Thomson, R.C. Blantz, Glomerulotubular balance, tubuloglomerular feedback, and salt homeostasis, J. Am. Soc. Nephrol. 19 (12) (2008) 2272–2275.

[10] Y.C. Hou, C.M. Zheng, T.H. Yen, et al., Molecular mechanisms of SGLT2 inhibitor on cardiorenal protection, Int J. Mol. Sci. 21 (21) (2020) 7833.

[11] C. Chu, D. Delić, J. Alber, M. Feger, Y. Xiong, T. Luo, A.A. Hasan, S. Zeng, M.M. S. Gaballa, X. Chen, L. Yin, T. Klein, S. Elitok, B.K. Krämer, M. Föller, B. Hocher, Head-to-head comparison of two SGLT-2 inhibitors on AKI outcomes in a rat ischemia-reperfusion model, Biomed. Pharm. 153 (2022), 113357, https://doi.org/10.1016/j.biopha.2022.113357.

[12] Y. Habib, B. Sm, D. Mbc, et al., The major molecular mechanisms mediating the renoprotective effects of SGLT2 inhibitors: an update, Biomed. Pharmacother. 120 (2019), 109526.

[13] S. Zeng, D. Denis, C. Chu, et al., Antifibrotic effects of low dose SGLT2 Inhibition with empagliflozin in comparison to Ang II receptor blockade with telmisartan in 5/6 nephrectomised rats on high salt diet, Biomed. Pharmacother. 146 (2021), 112606.

[14] M. Jiang, H. Chen, G. Guo, et al., Studying kidney diseases at the single-cell level, Kidney Dis. 7 (5) (2021) 335–342.

[15] F. Hildebrandt, Genetic kidney diseases, Lancet 375 (9722) (2010) 1287–1295.

[16] J. Yu, S. Mao, Y. Zhang, et al., MnTBAP therapy attenuates renal fibrosis in mice with 5/6 nephrectomy, Oxid. Med. Cell. Longev. (2016) 7496930.

[17] C.C. Yang, Y.T. Chen, C.G. Wallace, et al., Early administration of empagliflozin preserved heart function in cardiorenal syndrome in rat, Biomed. Pharm. 109 (2019) 658–670.

[18] S.V. Jabba, A. Oelke, R. Singh, et al., Macrophage invasion contributes to degeneration of stria vascularis in Pendred syndrome mouse model, BMC Med. 22 (2006) 37.

[19] L. Zhou, H. Zhuo, H. Ouyang, et al., Glycoprotein non-metastatic melanoma protein b (Gpnmb) is highly expressed in macrophages of acute injured kidney and promotes M2 macrophages polarization, Cell Immunol. 316 (2017) 53–60.

[20] P. Ramachandran, R. Dobie, J.R. Wilson-Kanamori, et al., Resolving the fibrotic niche of human liver cirrhosis at single-cell level, Nature 575 (7783) (2019) 512–518.

[21] R.K. Kasam, S. Ghandikota, D. Soundararajan, et al., Inhibition of aurora kinase B attenuates fibroblast activation and pulmonary fibrosis, EMBO Mol. Med. 12 (9) (2020), e12131.

[22] F. Wang, S. Zhang, I. Vuckovic, et al., Glycolytic stimulation is not a requirement for M2 macrophage differentiation, Cell Metab. 28 (3) (2018) 463–475.

[23] P.M. Tang, D.J. Nikolic-Paterson, H.Y. Lan, Macrophages: versatile players in renal inflammation and fibrosis, Nat. Rev. Nephrol. 15 (3) (2019) 144–158.

[24] V. Vielhauer, E. Berning, V. Eis, et al., CCR1 blockade reduces interstitial inflammation and fibrosis in mice with glomerulosclerosis and nephrotic syndrome, Kidney Int. 66 (6) (2004) 2264–2278.

[25] J. Li, H. Liu, S. Takagi, et al., Renal protective effects of empagliflozin via inhibition of EMT and aberrant glycolysis in proximal tubules, JCI Insight 5 (6) (2020), e129034.

[26] X. Liu, C. Xu, L. Xu, et al., Empagliflozin improves diabetic renal tubular injury by alleviating mitochondrial fission via AMPK/SP1/PGAM5 pathway, Metabolism 111 (2020), 154334.

[27] J. Li, X. Qu, J.F. Bertram, Endothelial-myofibroblast transition contributes to the early development of diabetic renal interstitial fibrosis in streptozotocin-induced diabetic mice, Am. J. Pathol. 175 (4) (2009) 1380–1388.

[28] L.L. Lv, P.M. Tang, C.J. Li, et al., The pattern recognition receptor, Mincle, is essential for maintaining the M1 macrophage phenotype in acute renal inflammation, Kidney Int. 91 (3) (2017) 587–602.

[29] H.J. Anders, B. Suarez-Alvarez, M. Grigorescu, et al., The macrophage phenotype and inflammasome component NLRP3 contributes to nephrocalcinosis-related chronic kidney disease independent from IL-1-mediated tissue injury, Kidney Int. 93 (3) (2018) 656–669.

[30] L. Tang, H. Zhang, C. Wang, et al., M2A and M2C macrophage subsets ameliorate inflammation and fibroproliferation in acute lung injury through interleukin 10 pathway, Shock 48 (1) (2017) 119–129.

[31] V.S. LeBleu, G. Taduri, J. O'Connell, et al., Origin and function of myofibroblasts in kidney fibrosis, Nature 19 (8) (2013) 1047–1053.

[32] Y.Y. Wang, H. Jiang, J. Pan, et al., Macrophage-to-myofibroblast transition contributes to Interstitial fibrosis in chronic renal allograft injury, J. Am. Soc. Nephrol. 28 (7) (2017) 2053–2067.

[33] X.M. Meng, S. Wang, X.R. Huang, et al., Inflammatory macrophages can transdifferentiate into myofibroblasts during renal fibrosis, Cell Death Dis. 7 (12) (2016), e2495.

[34] L. Xu, N. Nagata, G. Chen, et al., Empagliflozin reverses obesity and insulin resistance through fat browning and alternative macrophage activation in mice fed a high-fat diet, BMJ Open Diabetes Res. Care 7 (1) (2019), e000783.

[35] L. Xu, N. Nagata, M. Nagashimada, et al., SGLT2 Inhibition by empagliflozin promotes fat utilization and browning and attenuates inflammation and insulin resistance by polarizing M2 macrophages in diet-induced obese mice, EBioMedicine 20 (2017) 137–149.

[36] T.M. Lee, N.C. Chang, S.Z. Lin, Dapagliflozin, a selective SGLT2 Inhibitor, attenuated cardiac fibrosis by regulating the macrophage polarization via STAT3 signaling in infarcted rat hearts, Free Radic. Biol. Med. 104 (2017) 298–310.

[37] C. Cochain, E. Vafadarnejad, P. Arampatzi, Single-Cell RNA-Seq reveals the yranscriptional landscape and heterogeneity of aortic macrophages in murine atherosclerosis, Circ. Res. 122 (12) (2018) 1661–1674.

[38] M. Kiss, S. Van Gassen, K. Movahedi, et al., Myeloid cell heterogeneity in cancer: not a single cell alike, Cell Immunol. 330 (2018) 188–201.

[39] Y. Zhao, Y. Guo, Y. Jiang, et al., Mitophagy regulates macrophage phenotype in diabetic nephropathy rats, Biochem. Biophys. Res. Commun. 494 (2) (2017) 42–50.

[40] C.H. Hung, Y.C. Lin, Y.G. Tsai, et al., Acrylamide induces mitophagy and alters macrophage phenotype via reactive oxygen species generation, Int. J. Mol. Sci. 22 (4) (2021) 1683.

[41] K. Jiang, Y. Xu, D. Wang, et al., Cardioprotective mechanism of SGLT2 inhibitor against myocardial infarction is through reduction of autosis, Protein Cell (2021) 8.

[42] N. Nasiri-Ansari, C. Nikolopoulou, K. Papoutsi, et al., Empagliflozin Aattenuates non-alcoholic fatty liver disease (NAFLD) in high fat diet fed ApoE(-/-) mice by activating autophagy and reducing ER stress and apoptosis, Int. J. Mol. Sci. 22 (2) (2021) 818.

[43] A.I. Korbut, I.S. Taskaeva, N.P. Bgatova, et al., SGLT2 inhibitor empagliflozin and DPP4 inhibitor Linagliptin reactivate glomerular autophagy in db/db mice, a model of type 2 diabetes, Int. J. Mol. Sci. 21 (8) (2020) 2987.

[44] C. Rocher, D.K. Singla, SMAD-PI3K-Akt-mTOR pathway mediates BMP-7 polarization of monocytes into M2 macrophages, PLoS One 8 (12) (2013), e84009.

[45] L. Qing, J. Fu, P. Wu, et al., Metformin induces the M2 macrophage polarization to accelerate the wound healing via regulating AMPK/mTOR/NLRP3 inflammasome singling pathway, Am. J. Transl. Res. 11 (2) (2019) 655–668.

[46] G.D. Stanciu, R.N. Rusu, V. Bild, et al., Systemic actions of SGLT2 inhibition on chronic mTOR activation as a shared pathogenic mechanism between alzheimer's disease and diabetes, Biomedicines 9 (5) (2021) 576.

[47] X.F. Ding, G. Chen, Y. Liang, et al., Sodium-glucose co-transporter-2 (SGLT-2) inhibition reduces glucose uptake to induce breast cancer cell growth arrest through AMPK/mTOR pathway, Biomed. Pharm. 132 (2020), 110821.

[48] A. Kogot-Levin, L. Hinden, Y. Riahi, et al., Proximal tubule mTORC1 is a central player in the pathophysiology of diabetic nephropathy and its correction by SGLT2 inhibitors, Cell Rep. 32 (4) (2020), 107954.

[49] W.W. Yau, B.K. Singh, R. Lesmana, et al., Thyroid hormone (T3) stimulates brown adipose tissue activation via mitochondrial biogenesis and MTOR-mediated mitophagy, Autophagy 15 (1) (2019) 131–150.

[50] X. Zhang, I. Sergin, T.D. Evans, et al., High-protein diets increase cardiovascular risk by activating macrophage mTOR to suppress mitophagy, Nat. Metab. 2 (1) (2020) 110–125.